



HAL
open science

Wide Cross-species RNA-Seq Comparison Reveals Convergent Molecular Mechanisms Involved in Nickel Hyperaccumulation Across Dicotyledons

Vanesa Sanchez Garcia de La Torre, Clarisse Majorel-Loulergue, Guillem J. Rigaille, Dubiel A. Gonzalez, Ludivine Soubigou-Taconnat, Yohan Pillon, Louise Barreau, Sébastien Thomine, Bruno Fogliani, Valérie Burtet-Sarramegna, et al.

► To cite this version:

Vanesa Sanchez Garcia de La Torre, Clarisse Majorel-Loulergue, Guillem J. Rigaille, Dubiel A. Gonzalez, Ludivine Soubigou-Taconnat, et al.. Wide Cross-species RNA-Seq Comparison Reveals Convergent Molecular Mechanisms Involved in Nickel Hyperaccumulation Across Dicotyledons. *New Phytologist*, 2021, 229 (2), pp.994-1006. 10.1111/nph.16775 . hal-02890477

HAL Id: hal-02890477

<https://hal.science/hal-02890477v1>

Submitted on 20 Nov 2020

HAL is a multi-disciplinary open access archive for the deposit and dissemination of scientific research documents, whether they are published or not. The documents may come from teaching and research institutions in France or abroad, or from public or private research centers.

L'archive ouverte pluridisciplinaire **HAL**, est destinée au dépôt et à la diffusion de documents scientifiques de niveau recherche, publiés ou non, émanant des établissements d'enseignement et de recherche français ou étrangers, des laboratoires publics ou privés.



New Phytologist

Wide Cross-species RNA-Seq Comparison Reveals Convergent Molecular Mechanisms Involved in Nickel Hyperaccumulation Across Dicotyledons

Journal:	<i>New Phytologist</i>
Manuscript ID	NPH-MS-2020-32526.R1
Manuscript Type:	MS - Regular Manuscript
Date Submitted by the Author:	n/a
Complete List of Authors:	García de la Torre, Vanesa; I2BC, Cell Biology Majorel, Clarisse; Univesity of New Caledonia, ISEA Rigaill, Guillem; IPS2, PMIN; Université d'Evry Val d'Essonne, Laboratoire de Mathématiques at Modélisation d'Evry (LaMME) González, Dubiel; Universidad Agraria de La Habana (UNAH), Department of Biology Soubigou-Taconnat, Ludivine; Institute of Plant Sciences Paris-Saclay (IPS2), 91192 Pillon, Yohan; Institut de recherche pour le developpement, LSTM Barreau, Louise; I2BC, Cell Biology Thomine, Sébastien; CNRS, Institute for Integrative Biology of the Cell (I2BC) 1 Fogliani, Bruno; Institut Agronomique néo-Calédonien (IAC), Equipe ARBOREAL; Univesity of New Caledonia, ISEA Burtet-Sarramegna, Valerie; Univesity of New Caledonia, ISEA Merlot, Sylvain; CNRS, I2BC
Key Words:	Hyperaccumulator, Metal, Nickel, RNA-Seq, IREG/Ferroportin, Convergence, <i>Noccaea caerulescens</i>

SCHOLARONE™
Manuscripts

1 **Wide Cross-species RNA-Seq Comparison Reveals Convergent Molecular**
2 **Mechanisms Involved in Nickel Hyperaccumulation Across Dicotyledons**

3
4 Vanesa S. Garcia de la Torre^{1§}, Clarisse Majorel-Loulergue², Guillem J. Rigail^{3,4,5},
5 Dubiel A. Gonzalez⁶, Ludivine Soubigou-Taconnat^{3,5}, Yohan Pillon⁷, Louise Barreau¹,
6 Sébastien Thomine¹, Bruno Fogliani^{2,8}, Valérie Burtet-Sarramegna², Sylvain Merlot^{1*}

7
8 ¹*Université Paris-Saclay, CEA, CNRS, Institute for Integrative Biology of the Cell (I2BC),*
9 *91198, Gif-sur-Yvette, France.*

10 ²*Institute of Exact and Applied Sciences (ISEA), Université de la Nouvelle-Calédonie, BP*
11 *R4, 98851, Nouméa cedex, New Caledonia*

12 ³*Université Paris-Saclay, CNRS, INRAE, Univ Evry, Institute of Plant Sciences Paris-*
13 *Saclay (IPS2), 91405, Orsay, France.*

14 ⁴*Laboratoire de Mathématiques et Modélisation d'Evry (LaMME), Université d'Evry,*
15 *CNRS, ENSIIE, USC INRAE, 23 bvd de France, 91037, Evry cedex, France*

16 ⁵*Université de Paris, CNRS, INRAE, Institute of Plant Sciences Paris-Saclay (IPS2),*
17 *91405, Orsay, France*

18 ⁶*Universidad Agraria de La Habana (UNAH), Departamento de Biología, 32700,*
19 *Mayabeque, Cuba*

20 ⁷*Laboratoire des Symbioses Tropicales et Méditerranéennes (LSTM), IRD, INRAE,*
21 *CIRAD, Montpellier SupAgro, Univ. Montpellier, 34398, Montpellier cedex, France*

22 ⁸*Institut Agronomique néo-Calédonien (IAC), Equipe ARBOREAL, BP 73, 98890, Païta,*
23 *New Caledonia*

24
25 [§]Present address: Molecular Genetics and Physiology of Plants (MGPP), Faculty of
26 Biology and Biotechnology, Ruhr University Bochum, 44801 Bochum, Germany

27
28 ^{*}Corresponding author: sylvain.merlot@i2bc.paris-saclay.fr ; Phone: +33-169824642

30 **Total word count (w/o summary): 5903**

31 Summary: 198

32 Introduction: 802

33 Materials and Methods: 1822

34 Results: 1913

35 Discussion: 1366

36 Number of Figures: 5

37 Fig. 1, Fig. 2, Fig.5 should be published in color

38 Number of tables: 1

39 Supporting Information: Fig: 7; Notes: 1, Tables: 6.

40

41 Keywords: Hyperaccumulator, Metal, Nickel, RNA-Seq, IREG/Ferroportin,

42 Convergence, *Noccaea caerulescens*.

44 **Summary**

- 45 • The Anthropocene epoch is associated with the spreading of metals in the
46 environment increasing oxidative and genotoxic stress on organisms. Interestingly,
47 about 500 plant species growing on metalliferous soils acquired the capacity to
48 accumulate and tolerate tremendous amount of nickel in their shoots. The wide
49 phylogenetic distribution of these species suggests that nickel hyperaccumulation
50 evolved multiple times independently. However, the exact nature of these
51 mechanisms and whether they have been recruited convergently in distant species
52 is not known.
- 53 • To address these questions, we have developed a cross-species RNA-Seq approach
54 combining differential gene expression analysis and cluster of orthologous group
55 annotation to identify genes linked to nickel hyperaccumulation in distant plant
56 families.
- 57 • Our analysis reveals candidate orthologous genes encoding convergent function
58 involved in nickel hyperaccumulation, including the biosynthesis of specialized
59 metabolites and cell wall organization. Our data also point out that the high
60 expression of IREG/Ferroportin transporters recurrently emerged as a mechanism
61 involved in nickel hyperaccumulation in plants. We further provide genetic evidence
62 in the hyperaccumulator *Noccaea caerulescens* for the role of the NcIREG2
63 transporter in nickel sequestration in vacuoles.
- 64 • Our results provide molecular tools to better understand the mechanisms of nickel
65 hyperaccumulation and study their evolution in plants.

67 Introduction

68 Because of their chemical and biochemical properties, transition metals play
69 fundamental roles in living organisms. However, when present in excess in the
70 environment they induce adverse effects on biological systems producing oxidative and
71 genotoxic stresses or causing secondary deficiency of essential elements because of
72 competition (Waldron *et al.*, 2009; Andresen *et al.*, 2018). Even though they contain
73 metal levels toxic to most plant species, metalliferous soils of geogenic or anthropogenic
74 origin are colonized by specific floras adapted to these high concentrations of metals.
75 While the majority of metallophyte species exclude metals from their tissues, over 700
76 species have acquired the capacity to accumulate and tolerate tremendous amount of
77 metals in their shoot (van der Ent *et al.*, 2013; Reeves *et al.*, 2018). Plants
78 hyperaccumulating nickel (>1000 mg/kg shoot dry weight) represent, with around 520
79 species, the vast majority of metal hyperaccumulators (Reeves *et al.*, 2018), likely
80 because of the frequent occurrence of outcrops originating from ultramafic rocks,
81 including serpentine soils, in regions of high biodiversity such as Cuba, New Caledonia
82 or the Mediterranean basin. The large phylogenetic distribution of nickel
83 hyperaccumulators in various plant families further suggest that nickel
84 hyperaccumulation appeared independently several times during plant evolution
85 (Kramer, 2010; Cappa & Pilon-Smits, 2014). However, whether the mechanisms
86 allowing hyperaccumulation have been recruited convergently or are specific to different
87 plant families is still poorly known.

88 As for other metals, the hyperaccumulation of nickel requires very efficient uptake by the
89 roots, translocation of nickel to the shoot and its accumulation in leaf cells. The
90 hyperaccumulation of nickel in leaves requires strong detoxification mechanisms
91 involving antioxidant and metal-chelating molecules, as well as the sequestration of
92 nickel in specific compartments (Verbruggen *et al.*, 2009; Kramer, 2010; Clemens,
93 2019). In most of the cases, nickel is stored in the vacuoles of epidermal cells away from
94 photosynthetic tissues (Küpper *et al.*, 2001; Broadhurst *et al.*, 2004; Bidwell *et al.*, 2004;
95 Mesjasz-Przybylowicz *et al.*, 2016; van der Ent *et al.*, 2019), but nickel enrichment was
96 also observed in the apoplast and cell walls surrounding epidermal cells (Krämer *et al.*,
97 2000; Bidwell *et al.*, 2004; van der Ent *et al.*, 2019).

98 In the field of metal hyperaccumulation, most of the molecular studies have been focused
99 on the deciphering of zinc and cadmium accumulation in Brassicaceae species related
100 to *A. thaliana*. Genetic and transcriptomic studies performed on *Arabidopsis halleri* and
101 *Noccaea caerulescens* indicated that metal hyperaccumulation is associated with high
102 and constitutive expression of genes encoding metal transporters, enzymes involved in
103 the biosynthesis of metal chelators and proteins involved in oxidative stress responses

104 (Becher *et al.*, 2004; Dräger *et al.*, 2004; Weber *et al.*, 2004; Hammond *et al.*, 2006;
105 Shahzad *et al.*, 2010). In *A. halleri*, it was further shown that knocking down the
106 expression of the highly expressed *HEAVY METAL ATPASE 4* transporter gene reduces
107 zinc accumulation, thus demonstrating the essential role of *HMA4* in zinc
108 hyperaccumulation (Hanikenne *et al.*, 2008). These data indicated that metal
109 hyperaccumulation essentially evolved from a dysregulation of genes involved in basic
110 mechanisms of metal homeostasis.

111 Despite the essential role of nickel in plants to sustain the activity of urease, our
112 knowledge of the molecular mechanisms involved in nickel homeostasis is still scarce.
113 In *Arabidopsis thaliana*, members of the IRT/ZIP and IREG/Ferroportin transporter
114 families have been shown to play a role in nickel uptake and distribution (Schaaf *et al.*,
115 2006; Morrissey *et al.*, 2009; Nishida *et al.*, 2011). Furthermore, genes encoding
116 IREG/Ferroportin transporters have been shown to be expressed at higher levels in
117 nickel hyperaccumulators compared to related non-accumulators from the
118 Brassicaceae, Rubiaceae and Asteraceae families (Halimaa *et al.*, 2014; Merlot *et al.*,
119 2014; Meier *et al.*, 2018). A recent transcriptomic study performed in roots of the non-
120 accumulator *A. thaliana* revealed that high nickel treatment induces the downregulation
121 of genes associated with cell walls, suggesting that the response to high nickel targets
122 cell wall functions (Lešková *et al.*, 2019). In addition, several organic molecules,
123 including histidine, nicotianamine and organic acids, have been shown to form
124 complexes with nickel and have been proposed to play a role in hyperaccumulation
125 (Krämer *et al.*, 1996; Vacchina *et al.*, 2003; Callahan *et al.*, 2012). However, whether
126 these elements participate in the complex nickel hyperaccumulation trait still needs to be
127 supported by functional and genetic evidences.

128 Here, we have developed an RNA-Seq approach combining differential gene expression
129 analysis and cluster of orthologous group (COG) annotation to identify orthologous
130 genes that have been convergently selected in plants to support nickel
131 hyperaccumulation. Our cross-species comparative analysis performed on leaf
132 transcriptomes of a wide diversity of dicotyledon families reveals several COGs
133 associated with nickel hyperaccumulation including genes involved in metal transport,
134 the biosynthesis of specialized metabolites and cell wall organization. We further provide
135 genetic evidence in the nickel hyperaccumulator *Noccaea caerulea* that the
136 IREG/Ferroportin transporter NcIREG2 is involved in nickel sequestration into vacuoles.

138 **Material and Methods**

139 *Plant material and sample collection*

140 Leaves of nickel hyperaccumulator plants belonging to 5 distinct plant families (Jestrow
 141 *et al.*, 2012; Jaffré *et al.*, 2013; Borhidi *et al.*, 2016; Gonneau *et al.*, 2014), Brassicaceae
 142 [*Noccaea caerulescens* subsp. *firmiensis* (*Ncfi*)], Cunoniaceae [*Geissois pruinosa*
 143 (*Gpru*)], Euphorbiaceae [*Leucocroton havanensis* (*Lhav*)], Rubiaceae [*P. costivenia*
 144 (*Pcos*), *P. gabriellae* (*Pgab*), *Psychotria grandis* (*Pgra*)], Salicaceae [*Homalium*
 145 *kanaliense* (*Hkan*)], and leaves of related non-nickel hyperaccumulators, Brassicaceae
 146 [*N. caerulescens* 'Viviez' (*Ncviv*), *N. montana* (*Nmon*)], Cunoniaceae [*G. racemosa*
 147 (*Grac*)], Euphorbiaceae [*Lasiocroton microphyllus* (*Lmic*)], Rubiaceae [*P. revoluta*
 148 (*Prev*), *P. semperflorens* (*Psem*)], Salicaceae [*H. betulifolium* (*Hbet*)], were collected on
 149 individual plants growing in their natural environment and localized by GPS (Supporting
 150 Information Table S1). We complied with local regulation for the access to these genetic
 151 resources. For each sample, a fraction of leaves was washed with water and dried for
 152 elemental analysis, and the other fraction fixed on site with liquid N₂ (*Gpru*, *Grac*, *Pgab*,
 153 *Psem*) or with RNAlater (Sigma Aldrich) and stored at 4°C (*Ncfi*, *Ncviv*, *Nmon*, *Lhav*,
 154 *Lmic*, *Pcos*, *Pgra*, *Prev*, *Hkan*, *Hbet*). RNAlater was removed in the laboratory and leaves
 155 were immediately stored at -80°C before RNA extraction.

156 Additionally, to generate reference transcriptomes, *Ncfi* and *Nmon* were grown in
 157 hydroponic condition in a climatic chamber (9 h light, 150 µE.m⁻².s⁻¹, 21 °C/17 °C
 158 day/night, 70 % humidity) for 7 weeks using a modified Hoagland's solution (Lanquar *et*
 159 *al.*, 2010), containing 20 µM Fe-HBED (Van Iperen International) and 37.5 µM NiCl₂. *L.*
 160 *havanensis* seeds were cultured *in vitro* on Murashige & Skoog Agar medium
 161 supplemented with 3.2 mM NiSO₄, as described (Gonzalez & Matrella, 2013).

162 A specimen of *Cunonia capensis* (*Ccap*) was obtained from a specialized plant nursery
 163 (Ets. Railhet, France) and grown in a green-house on coconut coir supplemented with
 164 fertilizer.

165 *Phylogenetic analysis*

166 Phylogenetic trees of nickel hyperaccumulator and non-accumulator species were
 167 constructed with FigTree using the checklist of metal hyperaccumulators from (Reeves
 168 *et al.*, 2018), the APG III classification (Chase & Reveal, 2009) and the plant time-
 169 calibrated tree from (Magallón *et al.*, 2015). Phylogenetic analysis of IREG/FPN protein
 170 family was performed with CLC Genomics Workbench v20 software (Qiagen).

171 *RNA sequencing*

172 Total RNA from leaves was extracted with RNeasy Plant Mini kit (Qiagen) for *Noccaea*
 173 species, Qiagen hybrid method for woody plants for *Psychotria* species from Cuba

174 (Johnson *et al.*, 2012), CTAB-PVP method for *Geissois* and *Psychotria* species from
175 New Caledonia (Johnson *et al.*, 2012), and TRI Reagent (Sigma-Aldrich) for
176 *Leucocroton*, *Lasiocroton* and *Homalium* species. DNA was removed from all RNA
177 samples by RNeasy Plant Mini kit on-column DNase I treatment.

178 RNA quality control, preparation of cDNA libraries, sequencing and raw reads processing
179 were performed by the POPS transcriptomic platform (IPS2, Orsay, France). Libraries
180 were prepared from 1 µg of total RNA using TruSeq Stranded mRNA kit (Illumina) and
181 sequenced with an Illumina HiSeq2000 sequencing system in 100bp paired-end mode.
182 Libraries meant to be directly compared were multiplexed and sequenced in a single run.
183 Adaptors and low-quality pair-end sequences were removed from the raw reads and the
184 ribosomal RNA was filtered using the SortMeRNA algorithm (Kopylova *et al.*, 2012). We
185 obtained between 27 and 106 million reads per libraries (Supporting Information Table
186 S2).

187 *De novo transcriptome assembly and annotation*

188 The transcriptome sequences of *Ncfi*, *Nmon*, *Pgab*, *Psem*, *Pgra*, *Pcos*, *Prev*, *Gpru*, *Grac*,
189 *Hkan*, *Hbet*, *Lhav* and *Lmic* were obtained independently by *de novo* assembly of paired-
190 end reads using CLC Genomics Workbench v9 software (Qiagen). A single library per
191 species was used to minimize genetic variability. Assembly parameters were set as
192 default, except similarity (0.95), length fraction (0.75) and the word size was optimized
193 for each sample (Supporting Information Table S2). The quality of *de novo* assemblies
194 was assessed by Transrate v1.0.3 using trimmed read sequences (Smith-Unna *et al.*,
195 2016) and BUSCO v4.0.4 using Viridiplantae odb10 lineage dataset (Simão *et al.*,
196 2015). The sequences of the resulting contigs were blasted (Blastx, E-value of $\leq 10E-6$)
197 against the Viridiplantae protein database (NCBI) and putative function annotated by
198 Gene Ontology (cut-off = 55; GO weight = -5) using Blast2GO (Conesa *et al.*, 2005).
199 Filtered contigs for length (≥ 200 nt) and expression (TPKM > 1) were translated for the
200 longest Open Reading Frame. Translated sequences longer than 20 amino acids,
201 together with *Arabidopsis thaliana* protein sequences (TAIR10, www.arabidopsis.org)
202 were analyzed by OrthoFinder to annotate Clusters of Orthologous Group (COG) (Emms
203 & Kelly, 2015).

204 *Differential gene expression analysis*

205 For each pair of species, read count estimation was carried out using CLC Genomics
206 Workbench v9 software by mapping sequencing reads of each sample replicate (default
207 parameters, except similarity: 0.875 and length fraction: 0.75) to the transcriptome of the
208 nickel hyperaccumulator species used as the reference. Statistical analyses to identify
209 Differentially Expressed Genes (DEGs) were performed using the edgeR Bioconductor

210 package (Robinson *et al.*, 2010). To examine transcript abundance, reads per kilobase
211 million (RPKM) were calculated. To evaluate the influence of the reference
212 transcriptome, we additionally performed swapping analyses using the transcriptome of
213 the non-accumulator species as reference (Supporting Information Table S2). The
214 association of contigs between transcriptomes of a pair of species was established by
215 reciprocal Blast.

216 *Multiple-testing analysis*

217 Following differential gene expression analyses, we recovered 25,313 COGs containing
218 at least one DEG and collected for each of these COG a number of test statistics (i.e. p-
219 value of all the contigs of this COG) per plant family. We further discarded COGs for
220 which we had test statistics for less than 3 plant families (15,052 COGs), and finally kept
221 10,261 COGs to perform the multiple-testing analysis using the Cherry R package
222 version 0.6-12 (Goeman *et al.*, 2018). We first provided the complete list of the
223 corresponding 121,133 p-values to Cherry and used the Simes inequality with the
224 hommelFast function in R. Then for every COG and plant family, we identified contigs
225 significantly up-regulated ($FC > 2$) and down-regulated and used Cherry to get a lower
226 bound on the number of H1 contigs (with a simultaneous 95% confidence using the
227 pickSimes function in R). For every COG, we counted the number of plant families with
228 at least one up-regulated contig (respectively down-regulated) identified by Cherry.
229 Finally, COGs containing up-regulated or down-regulated contigs in hyperaccumulators
230 species in at least 3 different plant families were selected as candidates COGs
231 associated with nickel hyperaccumulation.

232 *Molecular cloning*

233 Predicted full-length coding region of *NcflIREG2*, *GpruIREG1* and *LhavIREG2* were
234 amplified from leaf cDNAs of the corresponding species, using high-fidelity Phusion
235 polymerase (Thermo Scientific) with gene specific primers containing AttB recombination
236 sequences (Supporting Information Table S6). PCR products were first recombined into
237 pDONOR207 (Invitrogen) and then in pDR195-GTW or pMDC83 for expression in yeast
238 and *N. caerulescens* respectively (Curtis & Grossniklaus, 2003; Oomen *et al.*, 2008).

239 Artificial miRNA construct targeting *NcflIREG2* was designed using the WMD3-Web
240 microRNA Designer (<http://wmd3.weigelworld.org>). The amiRNA was engineered as
241 previously described (Schwab *et al.*, 2006), by PCR using the pRS300 backbone and
242 specific primers (Supporting Information Table S6). The *NcflIREG2*-amiRNA precursor
243 was recombined in pDONOR207 and then into the vector pK7GW2D (Karimi *et al.*,
244 2002). All constructs were confirmed by restriction analysis and sequencing.

245 *Functional analyses of IREG/Ferroportin in Saccharomyces cerevisiae*

246 IREG/Ferroportin coding regions cloned into pDR195-GTW, as well as pDR195-
247 AtIREG2 (Schaaf *et al.*, 2006), were transformed by the lithium acetate/PEG method into
248 the *Saccharomyces cerevisiae* BY4741 strain complemented by a functional *HIS3* gene.
249 Yeast sensitivity to nickel was scored by drop assay using serial dilution on histidine-free
250 YNB agar medium containing 20 mM MES (pH5.5), supplemented or not with NiCl₂.
251 Empty pDR195 vector was used as control. Experiments were repeated twice with three
252 independent transformants.

253 *Functional analysis of NcfiIREG2 in transgenic plants*

254 pK7GW2D-*NcfiIREG2-amiRNA* and pMDC83-*NcfiIREG2* were transformed into *N.*
255 *caerulescens* subsp. *firmiensis* by *Rhizobium rhizogenes* (Arqua1 strain) mediated *in*
256 *vitro* root transformation (Lin *et al.*, 2016). Transformed roots were selected using GFP
257 fluorescence under a Leica MZ FLIII Fluorescence Stereo Microscope. Non-transformed
258 roots were cut once a week until the whole root system was transgenic.

259 Independent lines transformed with pK7GW2D-*NcfiIREG2-amiRNA* were then
260 transferred in hydroponic culture as described above for a week and then with the
261 nutrient solution supplemented with 37.5 μM NiCl₂ for 4 weeks. For each transgenic line,
262 the root system was divided in two samples for RT-qPCR and elemental analysis.

263 *Elemental analysis*

264 Dried environmental leaf samples were mineralized by HNO₃. Multi-elemental analyses
265 were performed using ICP-AES (LAMA laboratory, IRD, New Caledonia) or MP-AES.

266 Plant samples from hydroponic cultures were washed twice with ice-cold 10 mM
267 Na₂EDTA and twice with ice-cold ultrapure water. Samples were dried at 65 °C for 16
268 hours, weighed and then digested with 70 % HNO₃ and H₂O₂ for a total of 8 h with
269 temperature ramping from 80 to 120 °C. Elemental analyses were performed using MP-
270 AES (Agilent 4200, Agilent Technologies) and metal concentration was calculated by
271 comparison with a metal standard solution.

272 *Confocal Imaging*

273 Roots transformed with pMDC83-*NcfiIREG2* were stained with 10 μg/ml propidium iodide
274 (PI) and imaged on a Leica SP8X inverted confocal microscope (IMAGERIE-Gif
275 platform) with laser excitation at 488 nm and collection of emitted light at 495–550 nm
276 for GFP and 600–650 nm for PI.

277 *Quantitative RT-PCR analyses*

278 Total RNA from *Noccaea* species was extracted with RNeasy Plant Mini kit or with TRI
279 Reagent for *Ncfi* transgenic roots. Total RNA from leaves of *Gpru* and *Ccap* was
280 extracted with the CTAB-PVP method as described above. DNA was removed from all

281 RNA samples by RNeasy Plant Mini kit on-column DNase I treatment. RNA (1 µg) were
282 converted to cDNA by random priming using SuperScript III or IV First-Strand reverse
283 transcriptase (Invitrogen) according to the manufacturer's instructions. Quantitative PCR
284 analysis were performed on a LightCycler 96 using LightCycler 480 SYBR Green I
285 Master Mix (Roche) with the following conditions: Initial denaturation (95 °C, 300 s),
286 followed by 40 cycles of amplification (95 °C, 15 s; 60 °C, 15 s; 72 °C, 15 s), and a
287 melting curve (95 °C, 10 s; 65 °C, 30 s and 95 °C, 1s). Sequence information for Ccap
288 (sample TIUZ) was obtained from the 1KP project (Matasci *et al.*, 2014). Reference
289 genes for *Noccaea species* (*6-phosphogluconate dehydrogenase decarboxylating 3*,
290 *Nc6PGDH*, Ncfi_contig_3009), and *Cunoniaceae species* (*Histone deacetylase 15*,
291 *GpruHDAC15*, Gpru_contig_14406) were selected from our RNA-Seq analyses. Specific
292 primers for *IREG/Ferroportin* and reference genes were designed to produce amplicons
293 of 100-200 nt (Supporting Information Table S6). Relative gene expression was
294 calculated using the primer efficiency correction method (Pfaffl, 2001). Two technical
295 replicates were used for each sample.

296 *General statistics*

297 Sample exploration and replication of sequencing data analysis were conducted using
298 limma R package (Ritchie *et al.*, 2015), correlation analyses were conducted by linear
299 regression using generic stats functions of R software and Heat-map clustering was
300 carried out using heatmap.2 function of the gplots R package (R Development Core
301 Team, 2015).

302 *Data availability*

303 Raw sequence files, read count files and *de novo* assembled transcriptomes are publicly
304 available in the NCBI's Gene Expression Omnibus under the SuperSeries accession
305 number GSE116054 or SubSeries accession numbers GSE115411 (Brassicaceae),
306 GSE116051 (Rubiaceae, New Caledonia), GSE116050 (Rubiaceae, Cuba),
307 GSE116048 (Cunoniaceae), GSE116052 (Salicaceae) and GSE116049
308 (Euphorbiaceae).

310 **Results**

311 *Sampling nickel hyperaccumulators from a wide diversity of plant families*

312 Nickel hyperaccumulators are found as herbaceous plants, shrubs or trees scattered in
313 50 plants families almost exclusively in eudicots (45 families), in both Rosids and
314 Asterids clades (Fig. 1). Some families such as Brassicaceae (87 taxons), Asteraceae
315 (45 taxons) and families of the COM clade comprising Cunoniaceae (48 taxons),
316 Euphorbiaceae (42 taxons) and Salicaceae (38 taxons) are enriched in nickel
317 hyperaccumulators (Jaffré *et al.*, 2013; Reeves *et al.*, 2018). The distribution of nickel
318 hyperaccumulators suggests that this complex trait appeared independently several
319 times during plant evolution but also that some families may have a predisposition to
320 develop this trait.

321 To cover this large diversity, we sampled leaves of 7 nickel hyperaccumulators from 5
322 genera (i.e. *Noccaea*, *Psychotria*, *Geissois*, *Homalium*, *Leucocroton*) corresponding to
323 Brassicaceae, Rubiaceae and the families of the COM clade Cunoniaceae, Salicaceae
324 and Euphorbiaceae. These samples have been collected in their natural environment on
325 ultramafic soils in France, New Caledonia and Cuba and the elemental analysis of these
326 samples confirmed the nickel hyperaccumulator status of the corresponding species. For
327 each hyperaccumulator, we also collected leaves of a closely related species or
328 accession not hyperaccumulating nickel (Table 1; Supporting Information Fig. S1, Table
329 S1). Both nickel hyperaccumulators and the corresponding non-hyperaccumulator
330 species were collected in the same geographic area, and when it was possible non-
331 hyperaccumulator species were collected on ultramafic soils (i.e. *N. montana*, *P.*
332 *semperflorens* and *H. betulifolium*).

334 *Identification of genes differentially expressed between hyperaccumulators and related* 335 *non-accumulators*

336 To identify genes differentially expressed between nickel hyperaccumulator and closely
337 related non-accumulator species, we performed RNA sequencing (RNA-Seq) using
338 Illumina paired-end technology (Supporting Information Fig. S2). In absence of genomic
339 reference sequences for these species, we assembled *de novo* the sequence of
340 expressed genes for 13 selected species using short paired-end Illumina reads. These
341 newly generated transcriptomes contain between 41,843 and 87,243 contigs for a total
342 assembly size ranging from 35 Mbp to 49 Mbp and a N50 ranging from 692 to 1735 bp
343 (Table 1, Supporting Information Table S2). With the exception of *N. montana*, these *de*
344 *novo* assemblies received a TransRate score ranging from 0.31 to 0.49 and the analysis
345 with BUSCO indicates that they contain from 61% to 89% of complete genes with 3% to

346 9% of missing genes (Supporting Information Table S2). These parameters indicate that
347 the quality of these *de novo* assemblies is in the range of the assemblies usually obtained
348 for plant transcriptomes with this sequencing technology. The significant higher number
349 of contigs and the lower scores obtained for *Noccaea montana* is likely the result of the
350 allogamous reproduction of *N. montana* increasing genetic diversity and thus affecting
351 *de novo* assembly. Subsequent annotation of these transcriptomes using Blastx
352 interrogation of Viridiplantae proteins database revealed significant homologies for 56 %
353 of the contigs on average (E-value $\leq 10E-6$). These annotated reference transcriptomes
354 constitute a unique and comprehensive resource for molecular studies on plant groups
355 of high interest.

356 The reads from each environmental sample replicates were then mapped to the nickel
357 hyperaccumulator reference transcriptome to identify differentially expressed (DE)
358 genes in 8 pairs of species (or accessions), each containing a hyperaccumulator and a
359 related non-accumulator. The fraction of DE genes ranged from 2 % to 29 % (Fold
360 Change ≥ 2 , *FDR* ≤ 0.05), depending on the pair of species considered (Fig. 2a;
361 Supporting Information Fig. S3, Table S4). To evaluate the influence of the choice of the
362 reference transcriptome, we performed swapping analysis. To perform this analysis, we
363 calculated the read count for each contig using the transcriptome of the non-accumulator
364 species as reference and we performed the same transcriptomic comparison as before.
365 We then compared the fold change of the contigs obtained with the hyperaccumulator
366 and the non-accumulator transcriptomes successively used as references (Supporting
367 Information Fig. S4). This analysis revealed that the results were strongly correlated in
368 most pair of species ($r = 0.81-0.85$; P-value < 0.05). The lower correlation ($r = 0.70$)
369 obtained when using the non-accumulator *N. montana* transcriptome as reference is
370 likely the result of the lower quality of the transcriptome assembly for this species.
371 Overall, the results indicated that the choice of the reference transcriptome when
372 studying closely related species had only a marginal influence on the identification of DE
373 genes.

374

375 *Identification of biological functions associated with nickel hyperaccumulation in distant* 376 *families*

377 To determine if dysregulated molecular and metabolic pathways are shared by nickel
378 hyperaccumulators from distant plant families, it was necessary to compare their
379 transcriptomes altogether with a functional emphasis. To this aim, we classified the gene
380 products into Clusters of Orthologous Groups (COG). Combining the 13 reference
381 transcriptomes, 443,400 contigs (66.5% of total) were assigned to 46,458 COGs

382 (Supporting Information Table S3), and 25,313 COGs included at least one DE gene in
383 one plant family. Following the differential gene expression analysis in the different plant
384 families, we performed a multiple-testing analysis at the COGs level using the R Cherry
385 package (Goeman & Solari, 2011). We selected up-regulated and down-regulated COGs
386 containing genes more expressed, and less expressed respectively, in
387 hyperaccumulators from at least 3 different plant families. This analysis revealed 26
388 groups, including 15 up-regulated COGs and 11 down-regulated COGs (Fig. **2b**;
389 Supporting Information Table S5). The functional annotation of these COGs indicated
390 that the most represented categories in up-regulated COGs (Fig. **2b, c**) correspond to
391 class I transposable elements (TEs), known as retrotransposons and to genes involved
392 in the biosynthesis and metabolism of specialized metabolites. In addition to organic
393 acids and nitrogen/oxygen ligands (e.g. histidine and nicotianamine acid) that are known
394 nickel ligands, more recent studies have highlighted the role of the phenylpropanoid
395 compounds coumarins and flavonoids as potential metal ligands involved in metal
396 transport, tolerance and accumulation in plants (Kasprzak *et al.*, 2015; Tsai & Schmidt,
397 2017; Corso *et al.*, 2018). Therefore, the high expression of genes coding for enzymes
398 involved in the biosynthesis of specific metabolites such as UDP-
399 glucose:anthocyanidin/flavonol 3-O-glucosyltransferase (COG 35) or BAHD
400 acyltransferase (COG 44) could therefore lead to an increased synthesis of metal ligands
401 in nickel hyperaccumulators.

402 On the other hand, the most represented categories in down-regulated COGs
403 correspond to genes involved in response to stress and in cell wall biogenesis or
404 organization (Fig. **2d**). This latter category includes COGs corresponding to expansin
405 (COG 75), xyloglucan endotransglucosylase/hydrolase (COG 109) and pectin
406 acetyltransferase (COG 423). Because of their capacity to bind positively charged metals,
407 cell walls may regulate the apoplastic mobility of metals or be a reservoir for metals in
408 nickel hyperaccumulators (Krämer *et al.*, 2000; Krzesłowska, 2011; Le Gall *et al.*, 2015).
409 However, it is difficult to predict the consequences of a reduced expression of these
410 genes on cell wall properties regarding metals binding in nickel hyperaccumulators.

411

412 *The high expression of IREG/Ferroportin transporters in leaves has a conserved function*
413 *in nickel hyperaccumulation*

414 Our analysis points to IREG/Ferroportin transporters (COG 1981) as some of the most
415 robustly up-regulated function associated with nickel hyperaccumulation in several plant
416 families (Fig. **2c**; Supporting Information Table S5). Phylogenetic analysis revealed that
417 Brassicaceae species, including *N. caerulescens*, contain 2 gene clusters, represented

418 by *A. thaliana* IREG1 and IREG2, belonging to COG 1981 (Supporting Information Fig.
419 S5). These transporters were shown to localize on different membranes and therefore
420 proposed to play distinct functions in metal transport (Schaaf *et al.*, 2006; Morrissey *et*
421 *al.*, 2009). In several species from the Euphorbiaceae, Salicaceae, Cunoniaceae and
422 Rubiaceae families, we also observe a duplication of IREG/Ferroportin genes. However,
423 these transporters do not cluster with AthaIREG1 or AthaIREG2 and it is therefore not
424 possible to infer their specific function. Genes encoding IREG/Ferroportin transporters
425 are significantly more expressed (from 4 to 800-fold increase) in several nickel
426 hyperaccumulator species from the Brassicaceae, Rubiaceae and Euphorbiaceae
427 families compared to their related non-accumulator species. Very recently, the high
428 expression in leaves of an IREG/Ferroportin gene from the Asteraceae species *Senecio*
429 *coronatus* was associated with the capacity to hyperaccumulate nickel (Meier *et al.*,
430 2018). Together, these results strongly support the hypothesis that the high expression
431 of *IREG/Ferroportin* in leaves may play an essential and conserved role in nickel
432 hyperaccumulation in a wide diversity of plant families in both Asterid and Rosid clades.

433 In the selected pairs of species of the Salicaceae and Cunoniaceae families originating
434 from New Caledonia, we did not detect differential expression of *IREG/Ferroportin* genes
435 (Fig. 2c). However, the analysis of our RNA-Seq data indicates that *IREG/Ferroportin*
436 genes are highly expressed in both hyperaccumulator and non-accumulator species
437 from these families compared to non-accumulators from Brassicaceae and
438 Euphorbiaceae families (Supporting Information Fig. S6a). Furthermore, the unique
439 *IREG/Ferroportin* gene (COG 1981) detected in the hyperaccumulator *Geissois pruinosa*
440 is 60-times more expressed than its orthologue in the non-accumulator Cunoniaceae
441 species *Cunonia capensis* from South Africa (Supporting Information Fig. S6b). The high
442 expression of *IREG/Ferroportin* genes in non-accumulator species endemic to New
443 Caledonia might be a genetic footprint of nickel tolerance and hyperaccumulation caused
444 by the recent (<35 Ma) colonization of this island then probably fully covered by an
445 ultramafic rock layer rich in nickel (Pillon *et al.*, 2010, 2014). After adaptive radiation,
446 some species that have colonized more recently exposed non-ultramafic areas might
447 have lost some of the important functions necessary for the full expression of the nickel
448 tolerance and hyperaccumulation traits while still expressing IREG/Ferroportin at high
449 levels.

450

451 *IREG/Ferroportin* transporters have a conserved function in vacuolar sequestration of
452 nickel in hyperaccumulators

453 To provide functional evidence for the conserved role of plant IREG/Ferroportin in nickel
454 hyperaccumulation, we expressed in yeast IREG/Ferroportin orthologs cloned from 3
455 nickel hyperaccumulators from the distant families Brassicaceae, Cunoniaceae and
456 Euphorbiaceae (Fig. 3). The expression of these transporters increases yeast resistance
457 to nickel. These results are consistent with a conserved function of plant
458 IREG/Ferroportin as metal exporters, driving nickel out of the cytosol in the extracellular
459 medium or in intracellular stores and thus reducing cytosolic toxicity.

460 We then wanted to investigate the biological function of IREG/Ferroportin in nickel
461 hyperaccumulation *in planta* using *Noccaea caerulescens* as a model. We chose to
462 target *NcIREG2*, the ortholog of *Arabidopsis thaliana* *IREG2*, because it shows the
463 strongest expression in both shoot and roots of the nickel hyperaccumulator *N.*
464 *caerulescens* subsp. *firmiensis* when compared with the non-accumulator *Noccaea*
465 *caerulescens* 'Viviez' (Fig. 4; Supporting Information Table S4). We first used *Rhizobium*
466 *rhizogenes* root transformation to express a C-terminal GFP tagged version of
467 *NcfilIREG2* in *N. caerulescens* subsp. *firmiensis*. *NcfilIREG2*-GFP is able to complement
468 the nickel hypersensitive phenotype of the *A. thaliana* *ireg2* mutant indicating that this
469 fusion protein is functional (Supporting Information Fig. S7). Confocal imaging of *N.*
470 *caerulescens* transgenic roots shows that *NcfilIREG2*-GFP localizes on the membrane
471 of the vacuole suggesting a role of this transporter in nickel storage in this intracellular
472 compartment (Fig. 5a). To support this hypothesis, we used the same transformation
473 strategy to silence the expression of *NcfilIREG2* using artificial amiRNA technology. We
474 generated 8 independent composite transgenic lines displaying different degrees of
475 *NcfilIREG2* silencing (Fig. 5b). Elemental analysis of these transgenic lines revealed a
476 decrease of nickel concentration in roots that strongly correlates ($R^2 = 0.97$, P-value <
477 0.001) with *NcfilIREG2* expression (Fig. 5c). In contrast, the concentration of nickel in the
478 shoots of these lines does not correlate with *NcfilIREG2* expression in roots ($R^2 = 0.45$).
479 Together, these results provide evidences that *NcfilIREG2* contributes to the
480 accumulation of nickel in the roots of *Noccaea caerulescens* subsp. *firmiensis* by driving
481 nickel sequestration in vacuoles. However, the expression of *NcIREG2* in roots does not
482 seem to be a limiting factor for the transport of nickel to the shoot in *N. caerulescens*
483 subsp. *firmiensis*.

485 Discussion

486 The development of RNA-Seq technologies has opened the possibility to study non-
487 model species at the molecular level. Yet, comparative biology has not fully benefited
488 from this revolution because of the difficulty to quantitatively compare transcriptomes
489 from distant species (Roux *et al.*, 2015). In this study, we have used a combination of
490 cross-species comparative transcriptomics analysis, COG annotation and multiple-
491 testing analysis to identify genes associated with nickel hyperaccumulation in a wide
492 diversity of plant families. While pairwise comparisons between a nickel
493 hyperaccumulator and a related non-hyperaccumulator species identified a high number
494 of candidate DE genes, it is expected that a large proportion of these candidate DE
495 genes are not directly linked to the nickel hyperaccumulation trait but also to other traits
496 differentiating these species. On the other hand, pairwise comparison of closely related
497 species or accessions with a distinctive hyperaccumulation phenotype may also fail to
498 reveal mechanisms involved in this multigenic trait as for example observed for IREG/
499 Ferroportin genes in *Geissois* species from New Caledonia (Fig. 2c, Fig. S6). Thus, we
500 focused our analyses on the identification of convergent mechanisms between families
501 (Fig. 2a; Supporting Information Fig. S3). This strategy allowed the identification of a
502 limited number of candidate DE genes playing a conserved function in nickel
503 hyperaccumulation. This strategy may fail to identify molecular mechanisms specific to
504 a group of plants (e.g. family, genus). However, a similar approach could likely be used
505 to identify such specific mechanisms but would require to increase the number of species
506 within this group.

507

508 The high expression of IREG/Ferroportin transporters was previously linked to nickel
509 hyperaccumulation in Brassicaceae and Asteraceae species (Halimaa *et al.*, 2014; Meier
510 *et al.*, 2018). Our results support these findings and further indicates that
511 IREG/Ferroportin transporters have been recurrently recruited as a convergent
512 mechanism for nickel hyperaccumulation in a wide diversity of plant species. It is also
513 interesting to notice that we did not identify other families of metals transporters
514 suggesting that, besides IREG/Ferroportin, diverse metal transporter families may have
515 been recruited to support other important steps of nickel accumulation in leaves of distant
516 hyperaccumulator species. Importantly, this result *a posteriori* validates our cross-
517 species comparative approach to identify genes playing a convergent role in nickel
518 hyperaccumulation.

519 Our results also point to a convergent role for several functions involved in the biogenesis
520 and organization of cell walls and in the synthesis of specialized metabolites (Fig. 2c,d).

521 The high expression of several genes involved in the metabolism of phenylpropanoid
522 compounds is linked to the hyperaccumulation trait in several families. Coumarins and
523 flavonoids have the capacity to bind metals and have been previously linked to iron
524 nutrition and cadmium accumulation (Kasprzak *et al.*, 2015; Tsai & Schmidt, 2017; Corso
525 *et al.*, 2018). These results suggest that nickel hyperaccumulators synthesize
526 specialized metabolites involved in the detoxification and transport of nickel. However,
527 the functional annotation of the selected COGs does not allow to pinpoint specific
528 pathways. Comparative metabolomic analyses of nickel hyperaccumulator and related
529 non-accumulator species may identify specialized metabolites associated with nickel
530 hyperaccumulation and therefore establish a direct link between identified COGs and
531 specialized metabolites biosynthetic pathways. A recent report showed that the excess
532 of nickel in *A. thaliana* leads to a reduced expression of genes associated with cell walls
533 of root cells (Lešková *et al.*, 2019). Accordingly, we observed a lower expression of
534 COGs associated with cell wall in several hyperaccumulator species. Interestingly, our
535 analysis also revealed the up-regulation of COG 19, corresponding to the cell wall-
536 associated kinase family (WAKL) in nickel hyperaccumulators (Fig. 2c). The expression
537 of members of the WAKL family has been shown to be induced by metals in plants and
538 the increased expression of *WAKL4* in *A. thaliana* increases tolerance to nickel (Hou *et*
539 *al.*, 2005). Together, these results suggest that a modification of the cell wall structure,
540 at least in specific tissues, could play a conserved role in nickel tolerance and
541 hyperaccumulation in plants.

542 We also identified several COGs corresponding to Class I retrotransposon up-regulated
543 in nickel hyperaccumulating species. The expression of these elements is known to be
544 responsive to stress conditions and their transposition can generate several types of
545 mutations that can result in the inactivation of gene function or in increased gene
546 expression by cis-addition (Casacuberta & González, 2013; Makarevitch *et al.*, 2015). In
547 the metal hyperaccumulator species *A. halleri*, Class I retrotransposons are linked to the
548 triplication of the *HMA4* gene and may account for the high expression of this metal
549 transporter essential for zinc hyperaccumulation (Hanikenne *et al.*, 2008). It is therefore
550 tempting to speculate that transposable elements are involved in the evolution of the
551 nickel hyperaccumulation trait by altering the activity of some important genes.

552

553 Although metal hyperaccumulators are not easily amenable to genetic engineering,
554 molecular genetic studies are necessary to demonstrate the role of candidate genes in
555 this complex trait (Hanikenne *et al.*, 2008). To support the essential role of
556 IREG/Ferroportin in nickel accumulation, we performed molecular and genetic studies in
557 roots of the hyperaccumulator *N. caerulescens subsp. firmiensis* (Fig. 5). These results

558 demonstrated that *NcIIREG2* localizes on the vacuole and that decreasing *NcIIREG2*
559 expression in roots strongly affects nickel accumulation (Fig. 5b). These results provide
560 a genetic evidence supporting a role of *NcIIREG2* in the storage of nickel in the vacuoles
561 of *N. caerulescens* cells. Surprisingly, the silencing of *NcIIREG2* in roots did not lead to
562 a significant increase in nickel accumulation in leaves (Fig. 5c). This result might appear
563 as counterintuitive because the sequestration of metals in root cells has been proposed
564 to be a factor limiting their translocation and therefore their accumulation in the shoot of
565 hyperaccumulators. Our results rather suggest that the expression of *NcIIREG2* in roots
566 of *N. caerulescens subsp. firmiensis* is not a factor limiting the hyperaccumulation of
567 nickel in leaves. This conclusion is further supported by the parallel comparison of
568 *NcIIREG2* expression and nickel accumulation in *N. caerulescens subsp. firmiensis* and
569 *N. caerulescens* 'Viviez'. This analysis indicates that there is no negative correlation
570 between the expression of *NcIIREG2* in roots and the capacity to accumulate nickel in
571 shoots (Fig. 4). This conclusion does not rule out that the expression of *NcIIREG2* in roots
572 may limit the translocation of nickel to shoots in other *Noccaea* accessions or species
573 such as *N. montana* (Fig. 4) or *N. japonica* as very recently proposed (Nishida *et al.*,
574 2020). In contrast, the high expression of *NcIIREG2* and the consecutive sequestration
575 of nickel in shoots might create a sink effect favoring the transfer of nickel from roots to
576 shoots in *N. caerulescens subsp. firmiensis*. To directly demonstrate the major role of
577 *NcIIREG2* in nickel hyperaccumulation, it will be necessary to further develop
578 transformation protocols of *N. caerulescens* to modify the expression of this gene in
579 shoots.

580 Based on our wide cross-species transcriptomic analysis and functional evidences
581 obtained in transgenic *N. caerulescens*, we propose that IREG/Ferroportin transporters
582 play a conserved and essential role in the storage of nickel in the vacuole of leaf cells in
583 a wide range of nickel hyperaccumulating species. This role was previously proposed for
584 the transporter PgIREG1 from the nickel hyperaccumulator *P. gabriellae* (Merlot *et al.*,
585 2014). However, we cannot completely exclude that some IREG/Ferroportin orthologues
586 differentially expressed in hyperaccumulators might localize on the plasma membrane
587 to transport nickel out of cells as this was proposed for the *A. thaliana* IREG1 transporter
588 (Morrissey *et al.*, 2009). In the context of nickel hyperaccumulation, these transporters
589 might facilitate cell-to-cell transport of nickel or transport nickel out of epidermal cells
590 leading to its accumulation in the cell walls (Krämer *et al.*, 2000; van der Ent *et al.*, 2019).
591 In the context of sustainable development, nickel hyperaccumulators are now viewed as
592 crops to extract and recycle metals from large areas of metalliferous soils (Grison, 2015;
593 Nkrumah *et al.*, 2016). As for other crops, we foresee that the molecular knowledge
594 obtained in our study could become instrumental for marker-assisted selection of

595 cultivars or molecular monitoring of agricultural practices to improve nickel
596 phytoextraction. This work provides a framework to identify additional key genes from
597 root transcriptomes involved in the efficient uptake and translocation of nickel to the
598 leaves. The identification of all molecular steps from uptake in roots to sequestration in
599 leaves is necessary to fully understand this complex trait.

For Peer Review

601 **Acknowledgments**

602 We thank professor Rosalina Berazaín Iturralde (JBN, Cuba) for invaluable information
603 on the Cuban flora, Louis-Charles Brinon (IAC, New Caledonia) for sample collection in
604 New Caledonia, Christelle Espagne for technical assistance, Véronique Brunaud and
605 Marie-Laure Martin-Magniette (IPS2, France) for guidance on *de novo* assembly and
606 biostatistical analysis, and Mark G. M. Aarts (WUR, Netherlands) for the *Noccaea* root
607 transformation protocol.

608 This work was supported by Grants ANR-13-ADAP-0004 (SM, BF, VBS) and CNRS Defi
609 Enviromics Gene-4-Chem to SM, a SCAC fellowship from the French Embassy in Cuba
610 to DAG and SM and an ATIGE grant from Genopole to GJR. This work has benefited
611 from the core facilities of Imagerie-Gif, a member of Infrastructures en Biologie Santé et
612 Agronomie (IBiSA), supported by France Biolmaging Grant ANR-10INBS-04-01 and the
613 Saclay Plant Science Labex Grant ANR-11-IDEX-0003-0. The POPS platform benefits
614 from the support of the LabEx Saclay Plant Sciences-SPS (ANR-10-LABX-0040-SPS).
615 We thank the South Province of New Caledonia and the Prefecture of Aveyron for plant
616 collection authorizations.

617

618 **Author contributions**

619 BF, VBS and SM designed the project; VSG, CML, DAG, BF, VBS and SM collected
620 plant samples; VSG, CML, DAG, LB performed experiments; LST supervised RNA-Seq
621 sequencing; VSG, GJR, YP, ST and SM analyzed the data; VSG, ST and SM wrote the
622 manuscript; all authors commented and approved the content of the manuscript.

624 **References**

- 625 **Andresen E, Peiter E, Kupper H. 2018.** Trace metal metabolism in plants. *Journal of*
626 *Experimental Botany* **69**: 909–954.
- 627 **Becher M, Talke IN, Krall L, Krämer U. 2004.** Cross-species microarray transcript
628 profiling reveals high constitutive expression of metal homeostasis genes in shoots of
629 the zinc hyperaccumulator *Arabidopsis halleri*. *Plant Journal* **37**: 251–268.
- 630 **Bidwell SD, Crawford SA, Woodrow IE, Sommer-Knudsen J, Marshall AT. 2004.**
631 Sub-cellular localization of Ni in the hyperaccumulator, *Hybanthus floribundus* (Lindley)
632 F. Muell. *Plant, Cell & Environment* **27**: 705–716.
- 633 **Borhidi AL, Oviedo-Prieto R, Fernández-Zequeira M. 2016.** Nuevos resultados de la
634 revisión taxonómica de los géneros *Palicourea* y *Psychotria* (Rubiaceae, Psuchotrieae)
635 en Cuba. *Acta Botanica Hungarica* **58**: 1–48.
- 636 **Broadhurst CL, Chaney RL, Angle JS, Erbe EF, Maugel TK. 2004.** Nickel localization
637 and response to increasing Ni soil levels in leaves of the Ni hyperaccumulator *Alyssum*
638 *murale*. *Plant and Soil* **265**: 225–242.
- 639 **Callahan DL, Roessner U, Dumontet V, De Livera AM, Doronila A, Baker AJ, Kolev**
640 **SD. 2012.** Elemental and metabolite profiling of nickel hyperaccumulators from New
641 Caledonia. *Phytochemistry* **81**: 80–89.
- 642 **Cappa JJ, Pilon-Smits EA. 2014.** Evolutionary aspects of elemental
643 hyperaccumulation. *Planta* **239**: 267–275.
- 644 **Casacuberta E, González J. 2013.** The impact of transposable elements in
645 environmental adaptation. *Molecular Ecology* **22**: 1503–1517.
- 646 **Chase MW, Reveal JL. 2009.** A phylogenetic classification of the land plants to
647 accompany APG III. *Botanical Journal of the Linnean Society* **161**: 122–127.
- 648 **Clemens S. 2019.** Metal ligands in micronutrient acquisition and homeostasis. *Plant,*
649 *Cell & Environment* **42**: 2902–2912.
- 650 **Conesa A, Götz S, García-Gómez JM, Terol J, Talón M, Robles M. 2005.** Blast2GO:
651 A universal tool for annotation, visualization and analysis in functional genomics
652 research. *Bioinformatics* **21**: 3674–3676.
- 653 **Corso M, Schvartzman MS, Guzzo F, Souard F, Malkowski E, Hanikenne M,**
654 **Verbruggen N. 2018.** Contrasting cadmium resistance strategies in two metalicolous
655 populations of *Arabidopsis halleri*. *New Phytologist* **218**: 283–297.
- 656 **Curtis MD, Grossniklaus U. 2003.** A Gateway Cloning Vector Set for High-Throughput
657 Functional Analysis of Genes in *Planta* **133** : 462–469.
- 658 **Dräger DB, Desbrosses-Fonrouge AG, Krach C, Chardonnens AN, Meyer RC,**
659 **Saumitou-Laprade P, Krämer U. 2004.** Two genes encoding *Arabidopsis halleri* MTP1

- 660 metal transport proteins co-segregate with zinc tolerance and account for high MTP1
661 transcript levels. *Plant J* **39**: 425–439.
- 662 **Emms DM, Kelly S. 2015.** OrthoFinder: solving fundamental biases in whole genome
663 comparisons dramatically improves orthogroup inference accuracy. *Genome Biology* **16**:
664 1–14.
- 665 **van der Ent A, Baker AJM, Reeves RD, Pollard AJ, Schat H. 2013.**
666 Hyperaccumulators of metal and metalloid trace elements: Facts and fiction. *Plant and*
667 *Soil* **362**: 319–334.
- 668 **van der Ent A, Spiers KM, Brueckner D, Echevarria G, Aarts MGM, Montargès-**
669 **Pelletier E. 2019.** Spatially-resolved localization and chemical speciation of nickel and
670 zinc in *Noccaea tymphaea* and *Bornmuellera emarginata*. *Metallomics* **11**: 2052–2065.
- 671 **Le Gall H, Philippe F, Domon J-M, Gillet F, Pelloux J, Rayon C. 2015.** Cell Wall
672 Metabolism in Response to Abiotic Stress. *Plants* **4**: 112–166.
- 673 **Goeman JJ, Solari A. 2011.** Multiple Testing for Exploratory Research. *Statistical*
674 *Science* **26**: 584–597.
- 675 **Goeman JJ, Solari A, Meijer RJ. 2019.** Cherry: Multiple testing methods for exploratory
676 research *R package version 0.6-13*.
- 677 **Gonneau C, Genevois N, Frerot H, Sirgucy C, Sterckeman T. 2014.** Variation of trace
678 metal accumulation, major nutrient uptake and growth parameters and their correlations
679 in 22 populations of *Noccaea caerulescens*. *Plant and Soil* **384**: 271–287.
- 680 **Gonzalez DA, Matrella S. 2013.** Nickel hyperaccumulation ‘in vitro’ by *Leucocroton*
681 *havanensis* (Euphorbiaceae). *Revista del Jardín Botánico Nacional* **34–35**: 83–88.
- 682 **Grison C. 2015.** Combining phytoextraction and ecocatalysis: a novel concept for
683 greener chemistry, an opportunity for remediation. *Environmental Science and Pollution*
684 *Research* **22**: 5589–5591.
- 685 **Halimaa P, Lin YF, Ahonen VH, Blande D, Clemens S, Gyenesei A, Haikio E,**
686 **Karenlampi SO, Laiho A, Aarts MG, et al. 2014.** Gene expression differences between
687 *Noccaea caerulescens* ecotypes help to identify candidate genes for metal
688 phytoremediation. *Environmental Science & Technology* **48**: 3344–3353.
- 689 **Hammond JP, Bowen H, White PJ, Mills V, Pyke KA, Baker AJM, Whiting SN, May**
690 **ST, Broadley MR. 2006.** A comparison of *Thlaspi caerulescens* and *Thlaspi arvense*
691 shoot transcriptomes. *New Phytologist* **170**: 239–260.
- 692 **Hanikenne M, Talke IN, Haydon MJ, Lanz C, Nolte A, Motte P, Kroymann J, Weigel**
693 **D, Krämer U. 2008.** Evolution of metal hyperaccumulation required cis-regulatory
694 changes and triplication of HMA4. *Nature* **453**: 391–395.
- 695 **Hou X, Tong H, Selby J, DeWitt J, Peng X, He Z-H. 2005.** Involvement of a Cell Wall-
696 Associated Kinase, WAKL4, in Arabidopsis Mineral Responses. *Plant Physiology* **139**:

- 697 1704–1716.
- 698 **Jaffré T, Pillon Y, Thomine S, Merlot S. 2013.** The metal hyperaccumulators from New
699 Caledonia can broaden our understanding of nickel accumulation in plants. *Frontiers in*
700 *plant science* **4**: 279.
- 701 **Jestrow B, Gutiérrez Amaro J, Francisco-Ortega J. 2012.** Islands within islands: A
702 molecular phylogenetic study of the *Leucocroton alliance* (Euphorbiaceae) across the
703 Caribbean Islands and within the serpentinite archipelago of Cuba. *Journal of*
704 *Biogeography* **39**: 452–464.
- 705 **Johnson MTJ, Carpenter EJ, Tian Z, Bruskiwich R, Burris JN, Carrigan CT, Chase**
706 **MW, Clarke ND, Covshoff S, DePamphilis CW, et al. 2012.** Evaluating Methods for
707 Isolating Total RNA and Predicting the Success of Sequencing Phylogenetically Diverse
708 Plant Transcriptomes. *PLoS ONE* **7**: e50226.
- 709 **Karimi M, Inzé D, Depicker A. 2002.** GATEWAY™ vectors for *Agrobacterium*-mediated
710 plant transformation. *Trends in Plant Science* **7**: 193–195.
- 711 **Kasprzak MM, Erxleben A, Ochocki J. 2015.** Properties and applications of flavonoid
712 metal complexes. *RSC Advances* **5**: 45853–45877.
- 713 **Kopylova E, Noé L, Touzet H. 2012.** SortMeRNA: Fast and accurate filtering of
714 ribosomal RNAs in metatranscriptomic data. *Bioinformatics* **28**: 3211–3217.
- 715 **Krämer U. 2010.** Metal hyperaccumulation in plants. *Annual Review of Plant Biology* **61**:
716 517–534.
- 717 **Krämer U, Cotter-Howells JD, Charnock JM, Baker AJM, Smith JAC. 1996.** Free
718 histidine as a metal chelator in plants that accumulate nickel. *Nature* **379**: 635–638.
- 719 **Krämer U, Pickering IJ, Prince RC, Raskin I, Salt DE. 2000.** Subcellular localization
720 and speciation of nickel in hyperaccumulator and non-accumulator *Thlaspi* species.
721 *Plant physiology* **122**: 1343–1353.
- 722 **Krzesłowska M. 2011.** The cell wall in plant cell response to trace metals:
723 polysaccharide remodeling and its role in defense strategy. *Acta Physiologiae Plantarum*
724 **33**: 35–51.
- 725 **Küpper H, Lombi E, Zhao FJ, Wieshammer G, McGrath SP. 2001.** Cellular
726 compartmentation of nickel in the hyperaccumulators *Alyssum lesbiacum*, *Alyssum*
727 *bertolonii* and *Thlaspi goesingense*. *J Exp Bot* **52**: 2291–2300.
- 728 **Lanquar V, Ramos MS, Lelièvre F, Barbier-Brygoo H, Krieger-Liszkay A, Krämer U,**
729 **Thomine S. 2010.** Export of Vacuolar Manganese by AtNRAMP3 and AtNRAMP4 Is
730 Required for Optimal Photosynthesis and Growth under Manganese Deficiency. *Plant*
731 *Physiology* **152**: 1986–1999.
- 732 **Lešková A, Zvarík M, Araya T, Giehl RFH. 2019.** Nickel Toxicity Targets Cell Wall-
733 Related Processes and PIN2-Mediated Auxin Transport to Inhibit Root Elongation and

- 734 Gravitropic Responses in Arabidopsis. *Plant and Cell Physiology* **0**: 1–17.
- 735 **Lin YF, Hassan Z, Talukdar S, Schat H, Aarts MG. 2016.** Expression of the ZNT1 Zinc
736 Transporter from the Metal Hyperaccumulator *Noccaea caerulescens* Confers
737 Enhanced Zinc and Cadmium Tolerance and Accumulation to *Arabidopsis thaliana*.
738 *PLoS ONE* **11**: e0149750.
- 739 **Magallón S, Gómez-Acevedo S, Sánchez-Reyes LL, Hernández-Hernández T. 2015.**
740 A metacalibrated time-tree documents the early rise of flowering plant phylogenetic
741 diversity. *New Phytologist* **207**: 437–453.
- 742 **Makarevitch I, Waters AJ, West PT, Stitzer M, Hirsch CN, Ross-Ibarra J, Springer
743 NM. 2015.** Transposable Elements Contribute to Activation of Maize Genes in Response
744 to Abiotic Stress. *PLOS Genetics* **11**: 1–12.
- 745 **Matasci N, Hung L, Yan Z, Carpenter EJ, Wickett NJ, Mirarab S, Nguyen N, Warnow
746 T, Ayyampalayam S, Barker M, et al. 2014.** Data access for the 1 , 000 Plants (1KP)
747 project. *GigaScience* **3**: 1–17.
- 748 **Meier SK, Adams N, Wolf M, Balkwill K, Muasya AM, Gehring CA, Bishop JM, Ingle
749 RA. 2018.** Comparative RNA-seq analysis of nickel hyperaccumulating and non-
750 accumulating populations of *Senecio coronatus* (Asteraceae). *The Plant Journal* **95**:
751 1023–1038.
- 752 **Merlot S, Hannibal L, Martins S, Martinelli L, Amir H, Lebrun M, Thomine S. 2014.**
753 The metal transporter PglREG1 from the hyperaccumulator *Psychotria gabriellae* is a
754 candidate gene for nickel tolerance and accumulation. *Journal of Experimental Botany*
755 **65**: 1551–1564.
- 756 **Mesjasz-Przybylowicz J, Przybylowicz W, Barnabas A, van der Ent A. 2016.**
757 Extreme nickel hyperaccumulation in the vascular tracts of the tree *Phyllanthus balgooyi*
758 from Borneo. *New Phytologist* **209**: 1513–1526.
- 759 **Morrissey J, Baxter IR, Lee J, Li L, Lahner B, Grotz N, Kaplan J, Salt DE, Gueriot
760 ML. 2009.** The ferroportin metal efflux proteins function in iron and cobalt homeostasis
761 in Arabidopsis. *Plant Cell* **21**: 3326–3338.
- 762 **Nishida S, Tsuzuki C, Kato A, Aisu A, Yoshida J, Mizuno T. 2011.** AtIRT1, the primary
763 iron uptake transporter in the root, mediates excess nickel accumulation in *Arabidopsis*
764 *thaliana*. *Plant Cell Physiology* **52**: 1433–1442.
- 765 **Nishida S, Tanikawa R, Ishida S, Yoshida J, Mizuno T, Nakanishi H, Furuta N. 2020.**
766 Elevated Expression of Vacuolar Nickel Transporter Gene IREG2 Is Associated With
767 Reduced Root-to-Shoot Nickel Translocation in *Noccaea japonica*. *Frontiers in Plant*
768 *Science* **11**: 610.
- 769 **Nkrumah PN, Baker AJM, Chaney RL, Erskine PD, Echevarria G, Morel JL, van der
770 Ent A. 2016.** Current status and challenges in developing nickel phytomining: an

- 771 agronomic perspective. *Plant and Soil* **406**: 1–15.
- 772 **Oomen R, Wu J, Lelièvre F, Blanchet S, Richaud P, Barbier-brygoo H, Aarts MGM,**
773 **Thomine S. 2008.** Functional characterization of NRAMP3 and NRAMP4 from the metal
774 hyperaccumulator *Thlaspi caerulescens*. *New Phytologist* **181**: 637–650.
- 775 **Pfaffl MW. 2001.** A new mathematical model for relative quantification in real-time RT-
776 PCR. *Nucleic Acid Research* **29**: 16–21.
- 777 **Pillon Y, Hopkins HC, Rigault F, Jaffre T, Stacy EA. 2014.** Cryptic adaptive radiation
778 in tropical forest trees in New Caledonia. *New Phytologist* **202**: 521–530.
- 779 **Pillon Y, Munzinger J, Amir H, Lebrun M. 2010.** Ultramafic soils and species sorting
780 in the flora of New Caledonia. *Journal of Ecology* **98**: 1108–1116.
- 781 **R Development Core Team. 2015.** R: A Language and Environment for Statistical
782 Computing. *R foundation for Statistical Computing*: <http://www.R-project.org/>.
- 783 **Reeves RD, Baker AJM, Jaffré T, Erskine PD, Echevarria G, van der Ent A. 2018.** A
784 global database for plants that hyperaccumulate metal and metalloid trace elements.
785 *New Phytologist* **218**: 407–411.
- 786 **Ritchie ME, Phipson B, Wu D, Hu Y, Law CW, Shi W, Smyth GK. 2015.** limma powers
787 differential expression analyses for RNA-sequencing and microarray studies. *Nucleic*
788 *Acid Research* **43**: e47.
- 789 **Robinson MD, McCarthy DJ, Smyth GK. 2010.** edgeR: A Bioconductor package for
790 differential expression analysis of digital gene expression data. *Bioinformatics* **26**: 139–
791 140.
- 792 **Roux J, Rosikiewicz M, Robinson-Rechavi M. 2015.** What to compare and how:
793 Comparative transcriptomics for Evo-Devo (M Robinson-Rechavi, Ed.). *Journal of*
794 *Experimental Zoology. Part B, Molecular and Developmental Evolution* **324**: 372–382.
- 795 **Schaaf G, Honsbein A, Meda AR, Kirchner S, Wipf D, von Wiren N. 2006.** *AtIREG2*
796 encodes a tonoplast transport protein involved in iron-dependent nickel detoxification in
797 *Arabidopsis thaliana* roots. *Journal of Biological Chemistry* **281**: 25532–25540.
- 798 **Schwab R, Ossowski S, Riester M, Warthmann N, Weigel D. 2006.** Highly Specific
799 Gene Silencing by Artificial MicroRNAs in *Arabidopsis*. *The Plant Cell* **18**: 1121–1133.
- 800 **Shahzad Z, Gosti F, Frérot H, Lacombe E, Roosens N, Saumitou-Laprade P,**
801 **Berthomieu P. 2010.** The five *AhMTP1* zinc transporters undergo different evolutionary
802 fates towards adaptive evolution to zinc tolerance in *Arabidopsis halleri*. *PLoS Genetics*
803 **6**: e1000911.
- 804 **Simão FA, Waterhouse RM, Ioannidis P, Kriventseva E V, Zdobnov EM. 2015.**
805 BUSCO: assessing genome assembly and annotation completeness with single-copy
806 orthologs. *Bioinformatics* **31**: 3210–3212.

- 807 **Smith-Unna R, Bournnell C, Patro R, Hibberd J, Kelly S. 2016.** TransRate: reference
808 free quality assessment of de novo transcriptome assemblies. *Genome Research* **26**:
809 1134–1144.
- 810 **Tsai HH, Schmidt W. 2017.** Mobilization of Iron by Plant-Borne Coumarins. *Trends in*
811 *Plant Science* **22**: 538–548.
- 812 **Vacchina V, Mari S, Czernic P, Marques L, Pianelli K, Schaumlöffel D, Lebrun M,**
813 **Lobinski R. 2003.** Speciation of nickel in a hyperaccumulating plant by high-
814 performance liquid chromatography-inductively coupled plasma mass spectrometry and
815 electrospray MS/MS assisted by cloning using yeast complementation. *Analytical*
816 *Chemistry* **75**: 2740–2745.
- 817 **Verbruggen N, Hermans C, Schat H. 2009.** Molecular mechanisms of metal
818 hyperaccumulation in plants. *New Phytologist* **181**: 759–776.
- 819 **Waldron KJ, Rutherford JC, Ford D, Robinson NJ. 2009.** Metalloproteins and metal
820 sensing. *Nature* **460**: 823–830.
- 821 **Weber M, Harada E, Vess C, Roepenack-Lahaye E V, Clemens S. 2004.** Comparative
822 microarray analysis of *Arabidopsis thaliana* and *Arabidopsis halleri* roots identifies
823 nicotianamine synthase, a ZIP transporter and other genes as potential metal
824 hyperaccumulation factors. *Plant Journal* **37**: 269–281.

826 **Figure legends**

827 **Figure 1: Phylogenetic distribution of nickel hyperaccumulators.** Eudicots Plant
 828 families containing nickel hyperaccumulators are indicated in red on the phylogenetic
 829 tree. The drawings illustrate the plant families and genera containing nickel
 830 hyperaccumulators that we have sampled from France, New Caledonia and Cuba.

831 **Figure 2: Cross-family comparative transcriptomics and orthologous group**
 832 **annotation of genes convergently associated with nickel hyperaccumulation.** (a)
 833 Cross-species comparative transcriptomic reveals Differential Expressed (DE) genes
 834 between nickel hyperaccumulator species (black) and related non-nickel accumulators
 835 (grey). Genes (contigs) are plotted according to their mean level of expression (x-axis)
 836 and their differential expression (y-axis) in the pair of species. The numbers of significant
 837 DE (red and blue dots) and non-DE genes are indicated ($\log_2FC > 1$, $FDR < 0.05$). (b)
 838 Distribution of the 26 selected Cluster of Orthologous Groups (COGs) associated with
 839 nickel hyperaccumulation according to their predicted function and their level of
 840 expression in hyperaccumulators: COGs containing DE genes more expressed in nickel
 841 hyperaccumulators belonging to at least 3 distinct plant families (up-regulated COGs)
 842 are in red and COGs containing DE genes less expressed in nickel hyperaccumulators
 843 (down-regulated) are in blue. (c) Heat-maps of contigs associated with the selected
 844 COGs up-regulated in nickel hyperaccumulators from 5 distinct families. COGs
 845 corresponding to Class I transposable elements are not presented. (d) Heat-maps of
 846 contigs associated with down-regulated COGs. The color scale represents the
 847 expression Fold change of contigs in pairwise comparative analysis. The grey color
 848 represents the absence of contigs. Abbreviations: *Ncfi* (*Noccaea caerulescens* subsp.
 849 *firmiensis*), *Ncviv* (*N. caerulescens* 'Viviez'), *Nmon* (*N. montana*), *Pgra* (*Psychotria*
 850 *grandis*), *Prev* (*P. revoluta*), *Pcos* (*P. costivenia*), *Pgab* (*P. gabriellae*), *Psem* (*P.*
 851 *semperflorens*), *Gpru* (*Geissois pruinosa*), *Grac* (*G. racemosa*), *Hkan* (*Homalium*
 852 *kanaliense*), *Hbet* (*H. betulifolium*), *Lhav* (*Leucocroton havanensis*), *Lmic* (*Lasiocroton*
 853 *microphyllus*), IREG/FPN (Iron Regulated/ Ferroportin), UGT85A (UDP-
 854 glucose:anthocyanidin/flavonol 3-O-glucosyltransferase), BAHD (BAHD
 855 acyltransferase), CYP71 (Cytochrome P450 71), CYP704 (Cytochrome P450 704), FAR
 856 (Fatty acyl-CoA reductase), SCPL (Serine carboxypeptidase), SSL (Strictosidine
 857 synthase), WAKL (Wall associated receptor kinase like), GLP (Germin-like protein), COR
 858 (Cold regulated gene), EXPA (Expansin), XTH (Xyloglucan
 859 endotransglucosylase/hydrolase), PAE (Pectin acetylsterase), CESA (Cellulose
 860 synthase), MLP (Major latex protein), JMT (Jasmonic acid carboxyl methyltransferase),

861 GDSL (GDSL esterase/lipase), GULLO (L-gulonolactone oxidase), LTP (Bifunctional
 862 inhibitor/lipid-transfer protein), DUF642 (DUF642 domain containing protein) and TPS
 863 (Terpene synthase).

864 **Figure 3. Nickel sensitivity of yeast cells expressing plant IREG/Ferroportin**
 865 **transporters.** Yeast cells expressing IREG/Ferroportin transporters cloned from *A.*
 866 *thaliana*, *N. caerulescens subsp. firmiensis*, *G. pruinosa* and *L. havanensis* were plated
 867 at different dilutions on a medium containing a toxic concentration of nickel for the control
 868 line (transformed with pDR195 vector).

869 **Figure 4. Nickel accumulation and NcIREG2 expression in various accessions of**
 870 **Noccea species.** All plants were grown in hydroponic condition for 8 weeks in presence
 871 of 37.5 μM NiCl_2 . (a) Nickel accumulation was measured in roots and shoots of *Noccea*
 872 *caerulescens* 'Viviez' (*Ncviv*), *N. caerulescens subsp. firmiensis* (*Ncfi*) and *N. montana*
 873 (*Nmon*). Results are mean value \pm SD ($n = 3$ biological replicates). Letters denote
 874 significant differences between accessions, with lowercase for roots and uppercase for
 875 shoots (Tukey HSD test, $p < 0.05$). (b) Quantitative RT-PCR analysis of NcIREG2
 876 expression was performed on the same plants. *NcIREG2* expression was corrected
 877 using Nc6PGDH as a reference gene and normalized to 1 for the expression in *Ncviv*.
 878 Relative expression is displayed with a log₂ scale. Results are mean value \pm SD ($n = 3$
 879 biological replicates).

880 **Figure 5. Localization and silencing of the IREG/Ferroportin transporter NcfilREG2**
 881 (a) NcfilREG2 localizes on the vacuolar membrane in *N. caerulescens* cells. Confocal
 882 picture of a transgenic line expressing NcfilREG2-GFP (green) in root cells. Cell wall was
 883 stained with propidium iodide (magenta). The scale bar corresponds to 5 μm . (b)
 884 Silencing of the IREG/Ferroportin transporter *NcfilREG2* in roots of the nickel
 885 hyperaccumulator *N. caerulescens subsp. firmiensis* reduces nickel accumulation. The
 886 expression of *NcfilREG2* was quantified by RT-qPCR (black bars) in 8 amiRNA
 887 transgenic lines and control lines transformed with the pK7WG2D vector ($n=3$) growing
 888 in presence of 37.5 μM NiCl_2 for 4 weeks. *NcfilREG2* expression was corrected using
 889 *Ncfi6PGDH* as reference gene and normalized to 1 for the expression in control lines.
 890 Nickel concentration was measured in parallel in roots of the same lines by MP-AES
 891 (green bars). (c) Correlation analysis between *NcfilREG2* expression and nickel
 892 accumulation. The quadratic correlation model showed positive correlation ($R^2 = 0.97^{**}$,
 893 $P\text{-value} < 0.001$) between *NcfilREG2* expression and nickel accumulation in roots (black
 894 dots) and non-significant correlation ($R^2 = 0.45$) between *NcfilREG2* expression in roots
 895 and nickel accumulation in shoots (grey dots).

897 **Tables**898 **Table 1. De novo assembled transcriptomes of nickel hyperaccumulators and**
899 **related non-nickel accumulator species[§]**

Family/Species	[Ni] [#] (ppm)	Origin	Nbr. contigs	Assembly size (Mbp)	N50 (bp)
Brassicaceae - Noccaea					
<i>Noccaea caerulescens</i> <i>subsp. firmiensis</i> (<i>Ncfi</i>)	7580	France	41843	43.6	1735
<i>N. caerulescens</i> 'Viviez' (<i>Ncviv</i>)	239	France	na*	na*	na*
<i>N. montana</i> (<i>Nmon</i>)	916	France	87243	48.8	692
Rubiaceae - Psychotria					
<i>Psychotria gabriellae</i> (<i>Pgab</i>)	17618	New Caledonia	60899	45.5	1140
<i>P. semperflorens</i> (<i>Psem</i>)	34	New Caledonia	66755	49.8	1181
<i>P. grandis</i> (<i>Pgra</i>)	15176	Cuba	45143	36.8	1344
<i>P. costivenia</i> (<i>Pcos</i>)	1251 ^{&}	Cuba	46451	35.1	1240
<i>P. revoluta</i> (<i>Prev</i>)	131	Cuba	56754	44.0	1245
Cunoniaceae - Geissois					
<i>Geissois pruinosa</i> (<i>Gpru</i>)	6239	New Caledonia	54969	42.1	1243
<i>G. racemosa</i> (<i>Grac</i>)	132	New Caledonia	58386	43.7	1021
Salicaceae - Homalium					
<i>Homalium kanaliense</i> (<i>Hkan</i>)	6342	New Caledonia	52634	40.6	1259
<i>H. betulifolium</i> (<i>Hbet</i>)	275	New Caledonia	49962	39.0	1294
Euphorbiaceae – Adelleae tribe					
<i>Leucocroton havanensis</i> (<i>Lhav</i>)	14073	Cuba	58990	44.4	1206
<i>Lasiocroton microphyllus</i> (<i>Lmic</i>)	43	Cuba	52421	39.8	1244

900 [§] Details are provided in Supporting Information Table S1 and S2901 [#] Mean nickel concentration measured in leaves (n=2, Table S1)902 ^{*} not assembled: The transcriptome of *Ncfi* is used as a reference for *Ncviv*903 [&] Concentration likely underestimated because the samples were conserved in water-based RNA^{later}

905 **The following Supporting Information is available for this article:**

906 **Figure S1:** Estimated time-divergence between species used in this study

907 **Figure S2:** Workflow used for RNA-Seq analyses

908 **Figure S3:** Additional MA-plot representation of cross-species comparative
909 transcriptomic analyses

910 **Figure S4:** Effect of the choice of the reference transcriptome on the identification of
911 Differentially Expressed genes

912 **Figure S5:** Molecular phylogeny of the plant IREG/Ferroportin family

913 **Figure S6:** Expression of *IREG/Ferroportin* orthologs in *Homalium* and *Geissois* species

914 **Figure S7:** The NcflIREG2-GFP fusion protein is functional in *A. thaliana*

915 **Table S1:** Metadata associated with plant samples

916 **Table S2:** RNA-Seq sequencing, assembly and mapping statistics

917 **Table S3:** Cluster of Orthologous Group analysis metrics

918 **Table S4:** Differentially Expressed Genes analysis

919 **Table S5:** List of Cluster of Orthologous Group associated with nickel hyperaccumulation

920 **Table S6:** List of primers.

921 **Notes S1:** References for Supporting Information

922

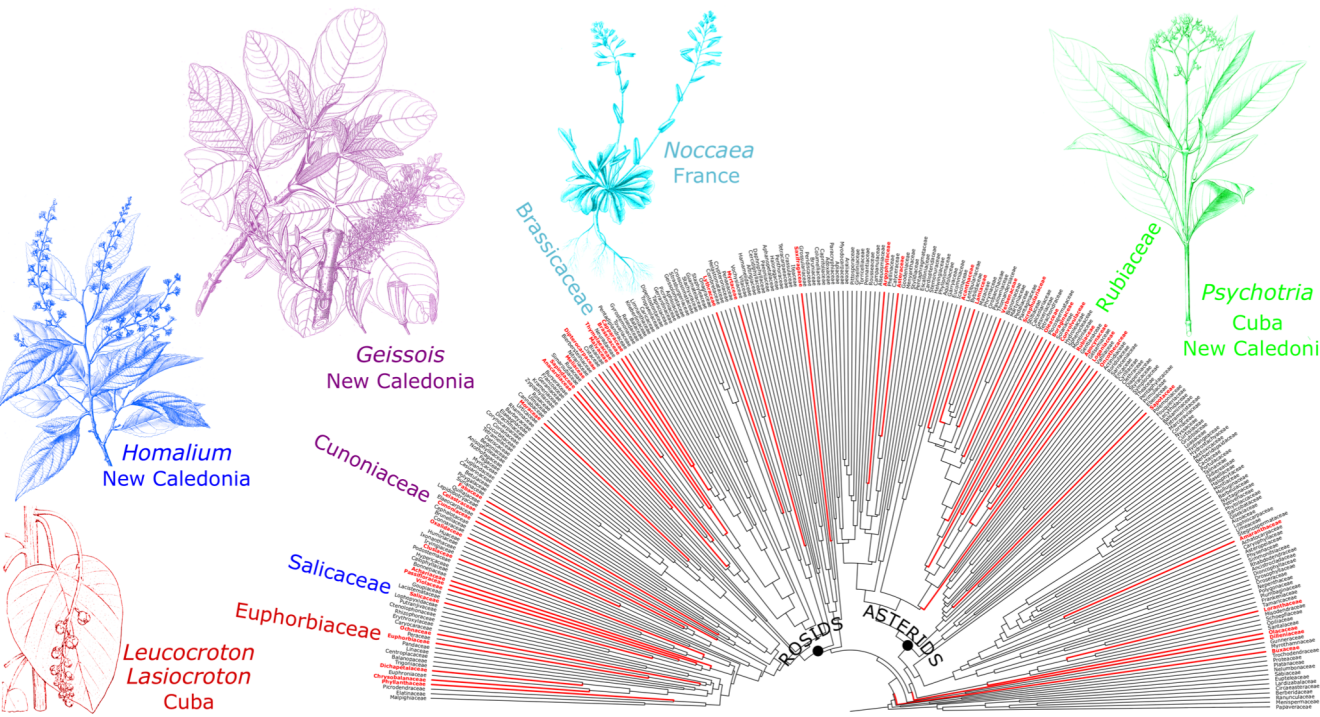
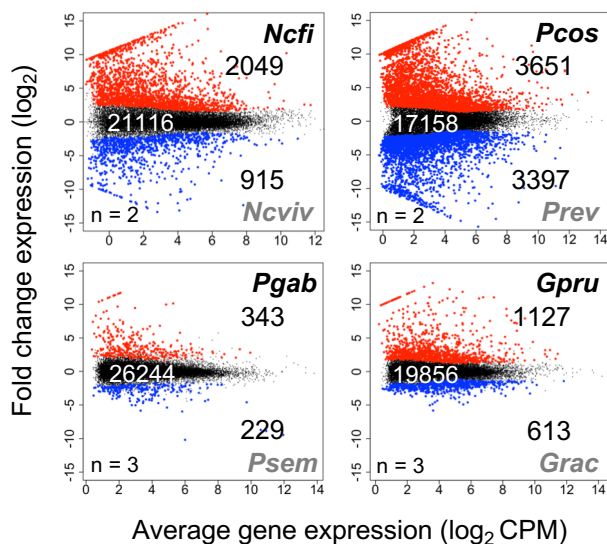
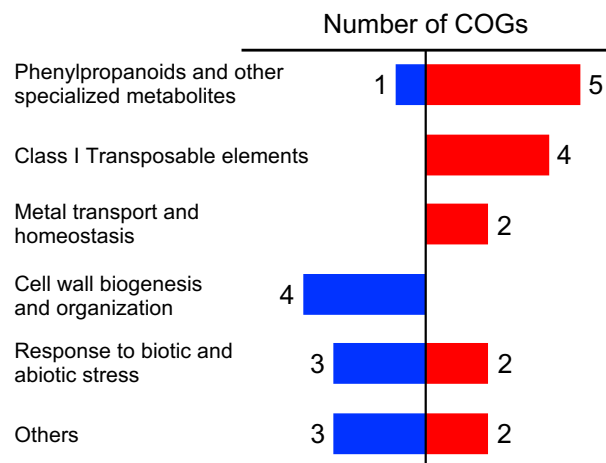


Figure 1

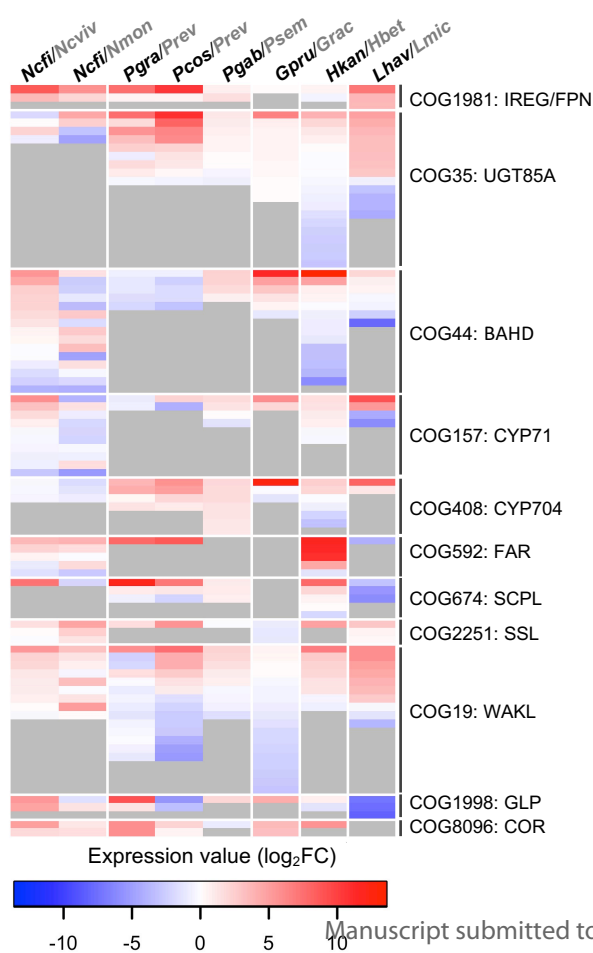
(a)



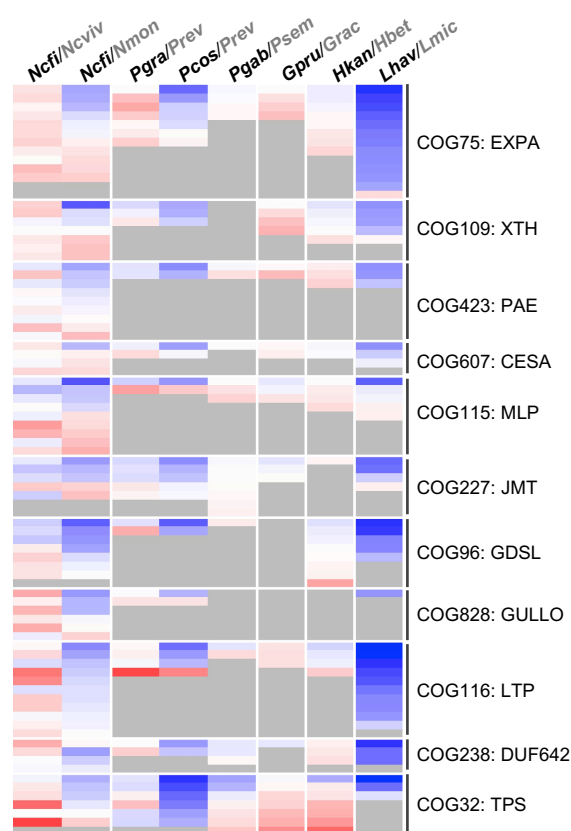
(b)



(c)



(d)



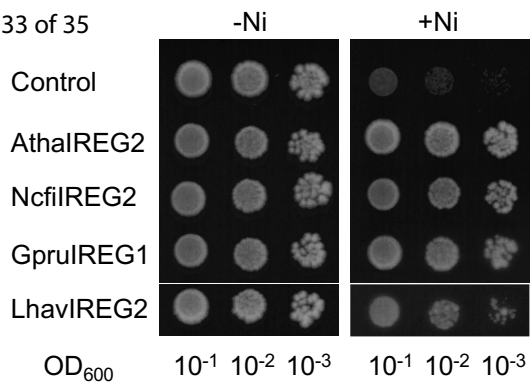
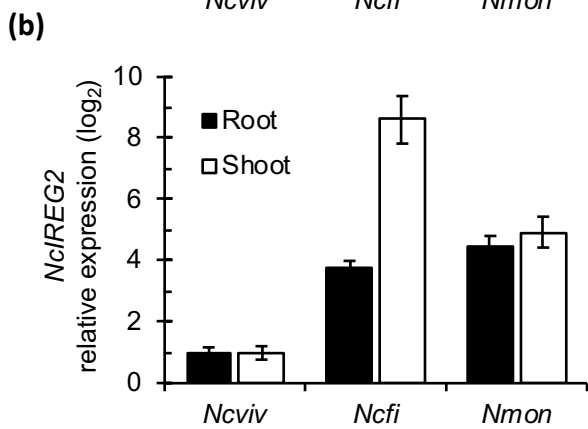
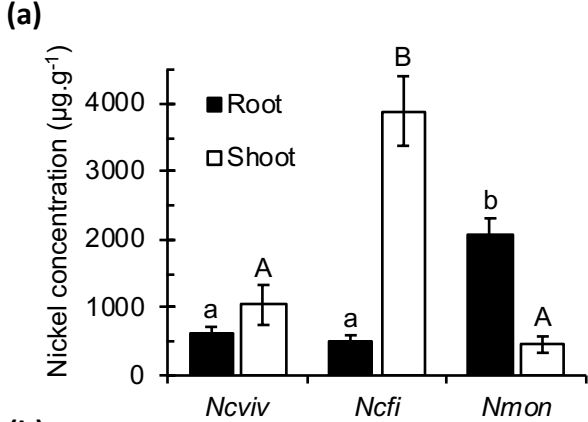


Figure 3



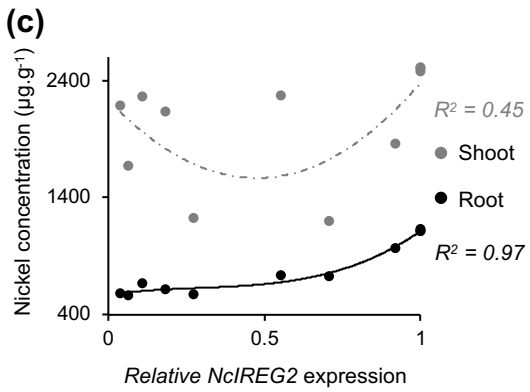
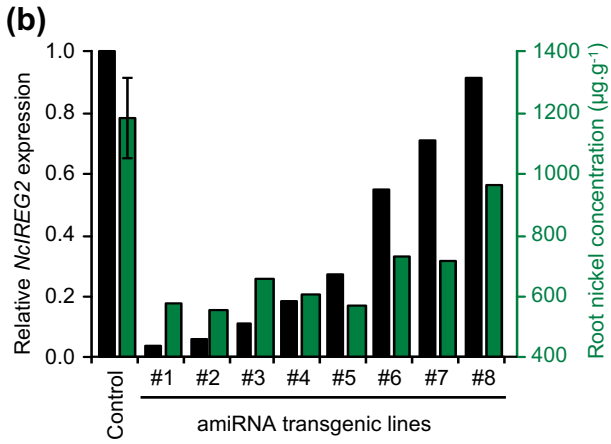
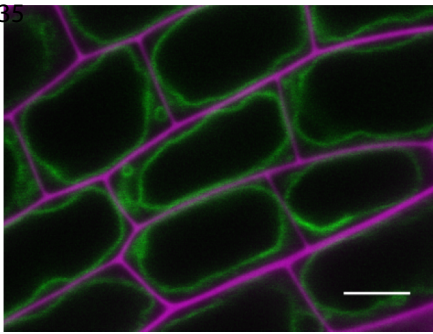


Figure 5